Sorsa, Olli; Romar, Henrik; Lassi, Ulla; Kallio, Tanja

Co-electrodeposited Mesoporous PtM (M=Co, Ni, Cu) as an Active Catalyst for Oxygen Reduction Reaction in a Polymer Electrolyte Membrane Fuel Cell

Published in:
Electrochimica Acta

DOI:
10.1016/j.electacta.2017.01.158

Published: 25/01/2017

Document Version
Peer-reviewed accepted author manuscript, also known as Final accepted manuscript or Post-print

Co-electrodeposited Mesoporous PtM (M=Co, Ni, Cu) as an Active Catalyst for Oxygen Reduction Reaction in a PEMFC

Olli Sorsa[1], Henrik Romar[2], Ulla Lassi[2],Tanja Kallio[1,*]

[1] *Department of Chemistry, Aalto University School of Chemical Technology, P.O. Box 16100, FI-00076 AALTO, Finland*

[2]*University of Oulu, Research Unit of Applied Chemistry, Talonpojankatu 2 B, FI-67100 KOKKOLA, Finland*

Abstract

Mesoporous thin films of PtCo, PtNi and PtCu are prepared by a single-step potentiostatic electrodeposition on a carbon substrate. Films are characterized by SEM, XRD, XRF and BET, and their activity for oxygen reduction reaction (ORR) is studied in an acidic three-electrode cell. The results are compared with both a commercial nanoparticle Pt/C catalyst and a Pt catalyst prepared using the same method. Additionally, the ORR activity of PtCo is studied in a fuel cell. The onset potential of ORR is found to be higher for all the electrodeposited catalysts compared to commercial Pt/C. The ORR activity of mesoporous Pt is found to be linearly dependent on the amount of deposited platinum within a platinum loading range of 0.1−0.5 mg cm^{-2}. All the mesoporous catalysts exhibited higher mass activity towards ORR than commercial Pt/C. Of the studied catalysts, PtCo is found to have the highest durability. Similar results are obtained in fuel cell experiments as PtCo exhibits enhanced durability and activity towards ORR, peak powers being 60, 70 and 90 mW g_{Pt}^{-1} for commercial Pt/C, mesoporous Pt and mesoporous PtCo, respectively.

Keywords: Fuel cells, Electrocatalysis, Oxygen reduction reaction, Electrodeposition, Mesoporous

* corresponding author Tanja Kallio
Tel. +358 50 5637567
E-mail tanja.kallio@aalto.fi

1 Introduction

Polymer electrolyte membrane fuel cells (PEMFCs) are considered as a sustainable method for producing electric power both in stationary and mobile applications. Once the energy of a renewable energy source (*e.g.* solar panel) is stored as hydrogen, it can be efficiently transformed to electricity in a fuel cell resulting in carbon neutral energy conversion cycle. The major limiting factor of a PEMFC is the low activity of cathode catalysts towards oxygen reduction reaction (ORR). [1] Platinum nanoparticles are currently the state-of-the-art catalyst for ORR. However, due to their relatively low ORR activity, high platinum loadings are still required to achieve moderate overall efficiency [2]. Platinum is considered as a critical raw material due to its low availability as well as political and economic problems related to its production. Consequently, the activity of platinum for ORR should be maximized to decrease the amount of platinum needed for PEMFCs.

To increase the activity of platinum, platinum alloys have been studied intensively for ORR since the 1970s [3, 4, 5]. The initial application of such catalysts was phosphoric acid fuel cells (PAFC), but later on it was discovered that similar catalysts are also active in PEMFCs. The most studied alloy catalysts for ORR in PEMFC are nanoparticle catalysts containing platinum as a noble metal and up to three first row transition metals as alloying metals; chromium, iron, cobalt and nickel being the most examined [6, 7, 8, 9, 10, 11, 12, 13]. The increase in the ORR activity of platinum is usually explained by a platinum skin and alloy core structure which decreases the distance between the platinum surface atoms [9, 14] and increases the d-electron vacancy of the platinum surface [8].

Nanoparticles are the smallest stable particles that can be produced from metals, and therefore exhibit the highest surface area to mass ratio. However, their durability is affected by catalyst dissolution and sintering caused by Ostwald ripening and migration [15]. Alloy catalysts have partially remedied these issues. The transition metal is more easily dissolved since it is less noble than platinum thus it increases the stability of platinum. Also, surface platinum atoms exhibit lower mobility in alloys, resulting in a lower rate for sintering [16]. By electrodeposition one can synthesize the active material directly on the membrane electrode assembly (MEA) of the fuel cell. A few methods have been developed for generating

high surface area metals by electrodeposition: using a size reducing agent such as an organic acid [17], using a template to deposit on [18] or electrodepositing by pulse current [19].

In addition to these methods, electrodeposition of metal thin films from a liquid crystalline phase has been studied since the late 1990s. Attard *et al*. [20, 21, 22] started the experiments on platinum and proved that its properties can be controlled by changing the conditions of the deposition. Later, mesoporous platinum synthetized using similar methods has been proven to be an active and relatively durable catalyst for oxygen reduction [23, 24, 25, 26, 27]. Compared to nanoparticles, less studies have been made on electrodeposited noble metal/transition metal alloy catalysts. For depositing multiple metals, one can either use co-electrodeposition as in this study or after electrodeposition of the less noble metals, dip the electrode in more noble metal so that the coating of the electrode occurs spontaneously [28].

Here we combine the bimetallic approach to improve the properties of platinum used for nanoparticles with the advantages of creating a porous layer of active material in a single step electrodeposition process. In contrast to most studies that compare their experimental results to a commercial Pt/C catalyst, we use two reference materials: a commercial Pt/C and a platinum catalyst prepared by electrodeposition. Cobalt, nickel and copper were chosen as the second metals because they are active for ORR as the volcano plot presented by Nørskov *et al.* [29] suggests and their electrodeposition is fairly easy to perform. Additionally, cobalt and nickel should form an ordered fcc-based cubic MPt_3 structure ($L1_2$) when alloyed with platinum at atomic ratios of platinum between 0.6 and 0.8. [30, 31]. Copper and platinum should form an ordered fcc-based rhombohedral CuPt structure ($L1_1$) at atomic ratios of platinum between 0.55 and 0.75 [32].

2 Experimental

2.1 Chemicals

For the electrodeposition, the following chemicals were used: Brij®C10 surfactant (Aldrich), hexachloroplatinic acid hydrate (HCPA, Aldrich), anhydrous cobalt (II) chloride (Freeport Cobalt), anhydrous nickel (II) chloride (Aldrich), copper (II) chloride dihydrate (VWR) and ultrapure ion-exchanged Milli-Q water (Millipore). For preliminary tests, a commercial Pt/C nanoparticle catalyst (20 *m* -% Pt, Alfa Aesar) was used as a reference material. For MEA preparation, 5 *m* -% Nafion® solution in lower aliphatic alcohols and water (Aldrich) was used as a binder, PtRu/C nanoparticle catalyst (40 *m* -% Pt, 20 *m* -% Ru, Alfa Aeasar) as the anode catalyst and Pt nanoparticle catalyst (20 *m* -% Pt, Alfa Aesar) as a reference material.

2.2 Electrodeposition

Liquid crystalline solutions of the metals were prepared by mixing the surfactant, water and HCPA and/or MCl_2 (M = Co, Ni, Cu) with a glass rod. Mixtures were heated in 40 °C for 30 min in a sealed vial and then stirred again. Finally, solutions were resealed for equilibration for at least 24 h before electrodeposition. The mixture contained 53 *m* -% BrijC10, 29 *m* -% water and 18 *m* -% metal salts. For PtCo and PtNi the molar ratio of Pt:M was 1:3 and for PtCu 3:1.

Carbon cloth with a gas diffusion layer (GDL) on one side and a microporous carbon layer on the other (GDL-CT, FuelCellsEtc) was used as a substrate for the electrodeposition. As a pretreatment, the substrate was immersed in 0.5 M H_2SO_4 for 1 h. For the electrodeposition, a thick layer of liquid crystalline solution was spread on the substrate covering an area of 1 cm^2. A platinum mesh was placed on the solution and pressed gently to ensure a proper connection between the substrate and the solution. The electrodeposition was performed at room temperature with a three-electrode system where the substrate served as a working electrode, the platinum mesh as a counter electrode and a saturated calomel electrode (SCE) Dri-ref (World Precision Instruments, Inc.) as a reference electrode.

Elliot *et al.* [22] have studied the effect of reduction potential of platinum in a similar matrix. Based on their results and previous studies done in our group [27], −0.2 V vs. SCE was selected here as the reduction potential for platinum because the film reduced at that potential has a high surface area and the efficiency of the reaction is relatively high. For bimetallic reduction, three different reduction potentials were used. The comparison can be seen in Table 2. Electrodeposition was performed at constant potential until the targeted amount of charge was transferred through the cell. Electrodeposition was performed using IviumStat XRi and IviumSoft as the software.

2.3 MEA preparation

For fuel cell measurements, platinum or a mixture of platinum and cobalt was electrodeposited on the carbon substrate with a geometric area of 5.29 cm^2. Nafion® solution was sprayed on the electrodeposited catalyst to achieve 0.5 mg cm^{-2} Nafion® content. Nafion® 115 membranes (Aldrich) were pretreated by boiling them first in 5 *m* -% H_2O_2, then in 0.5 M H_2SO_4 and finally multiple times in MQ water. Catalyst inks were prepared by mixing 75 *m* -% catalyst and 25 *m* -% Nafion in a mixture of *i*-PrOH and water with a magnetic stirrer and an ultrasonicator. Inks were painted on a pretreated membrane using an airbrush (Badger NO 100G) with nitrogen flow. Electrodeposited catalysts were heat pressed at 130 °C under 1 t for 2 min to form an MEA and the reference MEA was heat pressed at 130 °C under 5 t for 2 min. For all the MEAs, platinum loading was approximately 0.5 mg cm^{-2} for the cathodes and 2 mg cm^{-2} for the anodes.

2.4 Characterization

Scanning electron microscopy (SEM) with energy dispersive X-ray spectroscopy (EDX) was carried out using a JEOL JSM-7500F microscope. X-ray diffraction (XRD) was performed using a PANalytical X'PertPro diffractometer equipped with a Cu $K_{\alpha 1}$ X-ray source and X-ray fluorescence (XRF) using a PANalytical AXios mAX spectrometer.

2.5 Determination of specific surface areas and pore size distributions

Specific surface areas and pore size distributions were measured on a Micromeritics ASAP 2020 by adsorption of nitrogen. For the physisorption of nitrogen, approximately 100 mg of sample was weight

into a quartz tube. Prior to measurement, the samples were evacuated at 2 µm Hg at an elevated temperature (140 °C) in order to remove any contaminating gases from the samples. Surface areas were measured under isothermal conditions obtained by immersing the sample container into liquid nitrogen by addition of small portions of nitrogen. The specific surface areas were calculated according to the Brunauer-Emmet-Teller (BET) model [33]. Pore volumes and pore size distributions were calculated according to the Barret-Joyner-Halenda (BJH) model [34]. With the instrumental setup used, micropores down to 1.5 nm in diameter could be measured.

2.6 Electrochemical characterization

All the catalysts were measured using a conventional three-electrode cell. Additionally, activity of PtCo and Pt were investigated in a fuel cell.

In the three-electrode cell, a self-made reversible hydrogen electrode (RHE) was used as the reference electrode and a platinum wire as the counter electrode. The cell was thermostated at 25 °C and 0.5 M H_2SO_4 (Merck) was used as the electrolyte. The samples were immersed into the solution using a pocket made of polypropylene and attached to the working electrode using a graphite current collector. To determine the activity of the catalyst, linear sweep voltammetry (LSV) was applied from 1.2 to 0.2 V with a scan rate of 5 mV s^{-1} in saturated oxygen. Background current was measured in nitrogen and it was subtracted from the current measured in oxygen to determine the true catalytic activity for ORR. For durability tests, the cell was cycled in oxygen between 1.2 and 0.4 V with a scan rate of 100 mV s^{-1}. The activity was determined at the beginning of the experiments, after 500 cycles and after 3500 cycles by repeating the LSV measurement described above. The results are *iR*-corrected for which the resistance was determined using electrochemical impedance spectroscopy. As a reference material, Pt/C nanoparticle catalyst (20 *m* -%, Alfa Aesar) was painted on the carbon substrate using the same method as for the MEAs. This electrode was not heat-pressed because it was not attached to a membrane.

The fuel cell was assembled by placing PTFE treated diffusion layers (40 % wet proofing for anode and 60 % wet proofing for ref cathode, Ludlow Coated Products, Inc.) on top of the anode catalyst layer and clamping the cell with a torque of 10 Nm. Polarization curves were measured with a 1 M methanol flow of 2 cm^3 min^{-1} and oxygen flow of 200 cm^3 min^{-1} from open circuit voltage to 0.05 V with a scan rate of 0.5 mV s^{-1} at 70 °C. Impedance measurements were done at 0.5 V between 100 kHz and 0.1 Hz with

an amplitude of 5 mV. During the measurement, hydrogen feed to the anode was 200 cm^3 min^{-1} and oxygen feed to the cathode was 200 cm^3 min^{-1}. Durability was examined by cycling the cell between 0.3 V and 0.5 V with a scan rate of 50 mV s^{-1} and by finally recording a 65 h long constant voltage measurement at 0.3 V. Electrochemical characterization was performed using an AUTOLAB PGSTAT100 potentiostat equipped with GPES and FRA softwares.

3 Results and discussion

3.1 Electrodeposition

Linear sweep voltammetry was used to determine relevant potentials for the deposition of mesoporous structures. Linear sweeps of the studied bimetallic systems, PtCo, PtNi and PtCu, are presented in Figure 1 and the standard electrodeposition potentials in aqueous media in Table 1. Standard reduction values are potential values for the reaction when the activity of the active species is 1 in aqueous solution and consequently, are used here for comparing the reduction potential order in the liquid crystalline phase. For copper, the standard potential is higher than for cobalt and nickel as it is more noble metal. Also, the presence Cu^+ makes the situation more complex for copper. The sweeps show that the reduction of metals takes place at more positive potential when copper is present (Figure 1) which can be explained by either the presence of Cu^+ or chloride complexes. Due to the slow transfer process in the liquid crystalline phase, the reduction rate decreases rapidly and a local reduction current minimum is observed when platinum concentration is low (PtCo and PtNi). The metals are reduced simultaneously but the rate is low for nickel and cobalt as shown later in Table 2. At more negative potential, hydrogen evolution takes place and is the major cause of current increase.

Table 1. The standard reduction potentials of metals under study in aqueous media. [35]

Reaction	Standard potential / V
$(PtCl_6)^{2-}$ / $(PtCl_4)^{2-}$ + 2 Cl^-	0.680
$(PtCl_4)^{2-}$ / Pt + 4 Cl^-	0.755
Co^{2+} / Co	−0.280
Ni^{2+} / Ni	−0.257
Cu^{2+} / Cu	0.342
Cu^{2+} / Cu^+	0.159
Cu^+ / Cu	0.520

For PtCo and PtNi, the composition of the catalyst can be modified with two parameters: the electrolyte concentration and the applied potential. To minimize the amount of non-reacting platinum, a low platinum concentration and a high reduction potential were chosen. Also, the amount of evolved

hydrogen was minimized and therefore the controllability of the system increased when a more positive reduction potential was used. In the highly viscous liquid crystalline phase with a low platinum concentration the platinum reduction is limited by mass transfer so its reduction rate can be controlled by concentration. On the other hand, the transition metal reduction is limited by kinetics so its rate can be controlled by potential. Unfortunately, the system does not reach the limiting current during the electrodeposition, most probably because of the thick diffusion layer, therefore also the deposition time affects the composition of the product. Deposition time is dependent on the applied potential and on the desired charge.

For PtCu, because of the higher standard potential of copper in comparison to those of cobalt and nickel, the reduction potential has less effect on the composition of the bimetallic catalyst. Therefore, a higher platinum concentration must be used to achieve a similar molar ratio in the electrodeposit to PtNi and PtCo.

To investigate the composition and durability of the studied materials, XRF measurements were carried out before and after cycling the sample in a potential range of 0.4−1.2 V vs. RHE in a three-electrode cell. In Table 2, differences in the reduction potentials and their effect on the composition of the electrodeposits are compared. During the cycling, the amount of residual chlorides and the amount of less noble metals with respect to platinum have been reduced. This suggests that the loss of platinum is decreased and therefore the activity of the catalyst retained. When using a more positive electrodeposition potential, the amount of reduced platinum should increase [36]. This statement is roughly in agreement with the compositions given in Table 2. The reason could be related to mass transfer dynamics as the electrodeposition has been carried out in different potentials resulting in different deposition durations. Chlorides can be very harmful for platinum in electrocatalytical reduction of oxygen [37]. It must also be beard in mind that XRF is a semi-quantitative method.

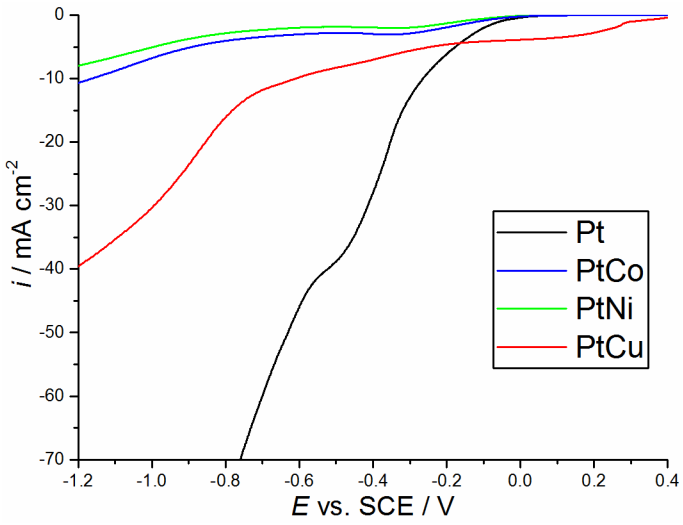

Figure 1. Linear sweep voltammograms for liquid crystalline solutions containing Pt, PtCo, PtNi and PtCu with a scan rate of 100 mV s^{-1}.

Table 2. The effect of the applied reduction potential on the metal composition and chlorine ratio before and after 3000 potential cycles. The compositions were measured with XRF and are given in molar units.

Sample	$E_{deposition}$ **vs. SCE / V**	**Initial**		**After 3000 cycles**	
		$\frac{Pt}{Pt+M}$	$\frac{Cl}{Pt+M}$	$\frac{Pt}{Pt+M}$	$\frac{Cl}{Pt+M}$
Pt	−0.20	1.00	2.6	1.00	0.6
PtCo	−0.35	0.61	1.7	0.77	0.5
	−0.40	0.61	1.5	0.80	0.4
	−0.45	0.58	2.5	-	-
PtNi	−0.35	0.64	2.2	0.80	0.5
	−0.40	0.51	5.3	0.77	0.5
	−0.45	0.47	8.0	-	-
PtCu	0.00	0.50	4.6	0.88	0.5
	−0.10	0.44	4.9	0.85	0.6
	−0.20	0.56	5.1	-	-

3.2 Characterization

SEM images (Figure 2) and EDX mappings (Figure 3) were produced to study the morphology of the catalyst and to ensure that the distribution of the metals is uniform. Electrodeposition generates particles with a diameter of 1−3 µm (Figure 2a) which start to agglomerate and later form a porous metal layer (Figure 2b). The layer does not lose its porosity when cycled in the electrochemical cell (Figure 2c) although its activity is reduced significantly as is shown below (Figure 6 and the related discussion). Cross section of a sample deposited on a gas diffusion layer is presented in Figure 2d. On the left hand side, the gas diffusion layer is observed, porous carbon layer is located in the middle and the electrodeposited metal layer is located on the right hand side, outlined in red. The average thickness of a layer containing 0.5 mg cm^{-2} platinum was estimated as 10 µm. The distributions of the metals in all the bimetallic catalysts were found to be uniform and the measured metal ratios are in agreement with the XRF results.

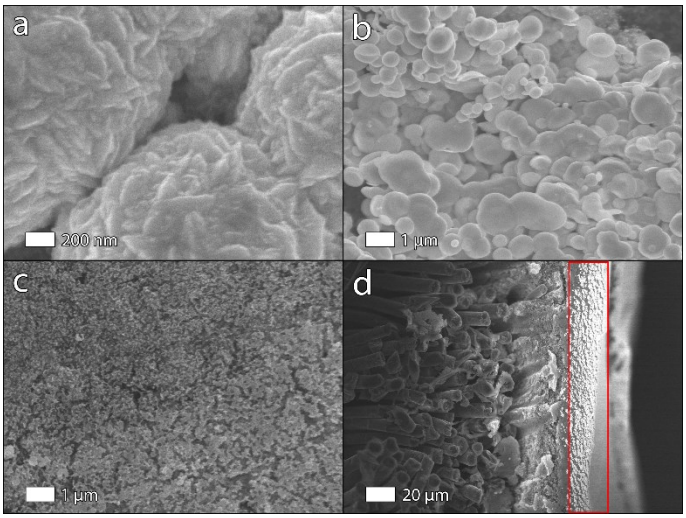

Figure 2. SEM images of the mesoporous catalysts: a) single particles, b) layer of particles, c) catalyst layer after cycling and d) cross section of the catalyst layer.

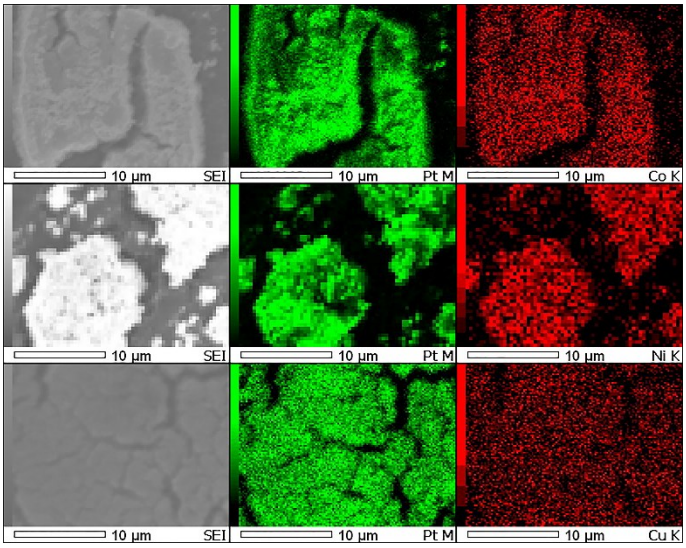

Figure 3. EDX maps of all the studied bimetallic catalysts.

To understand the surface morphology better, BET measurements were carried out for the studied catalysts. The pore size distribution and change in the BET area after 3000 potential cycles are presented in Table 3. The carbon substrate consists of mainly macropores, whereas the electrodeposited catalysts have almost equal amount of macropores and mesopores. Therefore, these catalyst layers can be considered mesoporous. Pores in mesosize range are considered to improve wettability and thus allow better ionic transfer in the pores [38] potentially enhancing ORR.

The total BET area of the commercial catalyst decreased 26 % after cycling whereas for the electrodeposited catalysts it remained the same or increased slightly. This predicts a high durability for the electrodeposited catalysts in a fuel cell as the layers can retain their porosity. Similar results have been published by Kibsgaard *et al.* [26] as the electrochemically active surface area (EASA) of their electrodeposited catalyst decreased 16 % during 10 000 potential cycles compared to commercial Pt/C nanoparticle catalyst showing a decrease of 53 %. The increase in the BET area of the electrodeposited PtM samples can be explained by dealloying of M. As Tables 1 and 2 show, cobalt, nickel and copper are more prone to dissolution which can increase the porosity of the electrocatalyst.

Table 3. The pore size distribution (determined by BJH) in the pristine samples and the change in the BET area after 3000 potential cycles of the studied catalyst and the carbon substrate. BET areas are in the range of 10 m^2 g^{-1} for all the samples.

Sample	Micropores $d < 2$ nm in V -%	Mesopores $2 < d < 50$ nm in V -%	Macropores $d > 50$ nm in V -%	% of BET area after cycling
Carbon Substrate	2	5	93	-
Pt/C	-	-	-	74
Pt	0	41	59	98
PtCo	1	44	55	108
PtNi	2	47	51	100
PtCu	1	45	54	133

XRD spectra of the studied catalysts and plain carbon paper are shown in Figure 4. Wide peaks at 25° and 40° are attributed to the carbon substrate. Narrow peaks at 18°, 37°, 42°, 72° and 75° are induced by polytetrafluoroethylene in the GDL. The platinum peaks are shifted in all the electrodeposited catalysts in comparison to the bulk platinum indicating a difference in the lattice parameters. The lattice parameter a for an fcc structure can be calculated using the Bragg's law

$$d = \frac{n\lambda}{2\sin\theta} \tag{1}$$

$$d_{hkl} = \frac{a}{\sqrt{h^2 + k^2 + l^2}} \tag{2}$$

where λ is the wavelength of the X-ray beam (1.5406 Å for Cu $K_{\alpha 1}$), θ is the diffraction angle and h, k and l the Miller indices. The shortest Pt-Pt distance can be calculated using the crystal geometry, which for an fcc structure is $a/\sqrt{2}$. The calculated lattice parameters and Pt-Pt distances are given in Table 4. All the catalysts have smaller lattice parameters than bulk platinum, 3.9236 Å [39]. This can be explained by form effects and contribution of transition metals. All the bimetallic catalysts have almost the same lattice parameter, 3.88 Å, and pure platinum catalysts have slightly higher, 3.90 Å. This is presumed to increase the ORR activity of platinum since the Pt-Pt distance has an optimum value of 2.6−2.7 Å for ORR [40]. Intensity of the platinum peaks is also different for different catalysts. Electrodeposited Pt has clearly the strongest platinum reflections but when comparing planes (111) and (200), PtNi shows weaker

peaks than PtCo and PtCu. This can be due to low metal loading, low crystallinity and small crystal grain size.

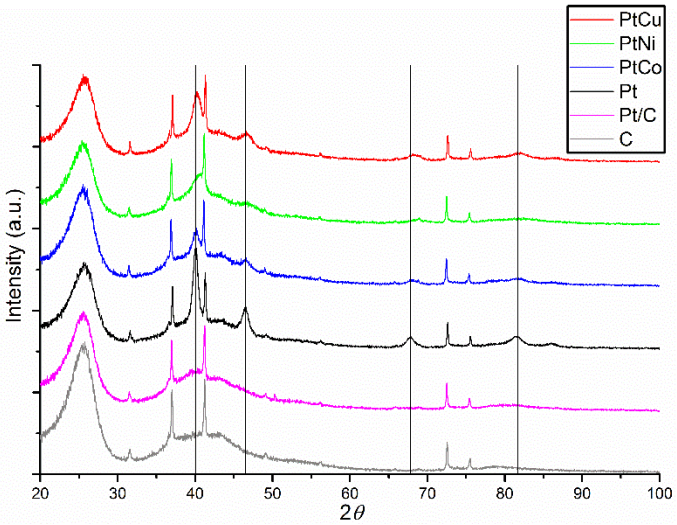

Figure 4. XRD patterns of electrodeposited Pt, PtCo, PtNi, PtCu, commercial Pt/C and the carbon substrate C. Vertical lines represent the reflections of electrodeposited platinum, from left to right planes (111), (200), (220) and (311).

Table 4. XRD angles, lattice parameters *a* and Pt-Pt distances for the studied catalysts calculated from planes (111) and (200).

Catalyst	**Plane**	**2θ / °**	***a* / Å**	**d_{Pt-Pt} / Å**
Pt/C	(111)	40.21	3.881	2.75
	(200)	46.56	3.898	
Pt	(111)	40.04	3.897	2.76
	(200)	46.55	3.899	
PtCo	(111)	40.18	3.884	2.75
	(200)	46.64	3.892	
PtNi	(111)	40.26	3.877	2.74
	(200)	46.72	3.886	
PtCu	(111)	40.26	3.877	2.74
	(200)	46.70	3.887	

The ORR measurements were done by immersing the catalyst deposited on the substrate in 0.5 M aqueous H_2SO_4. CVs in oxygen and nitrogen saturated electrolytes with a scan rate of 50 mV s^{-1} are presented in Figure 5a for the electrodeposited platinum. Due to the gas diffusion layer and porous carbon layer beneath the active material, mass transfer limited region is not observed for ORR. The carbon layer stores oxygen and feeds it to the catalyst, akin to operation in a fuel cell. Therefore, the system was under kinetic control for the linear sweeps done even with a relatively slow scan rate of 5 mV s^{-1}. Also, it was found that the ORR activity of the catalyst was linearly dependent on the amount of platinum reduced, in the range of 0.1−0.5 mg Pt cm^{-2} (not shown). Thus, the results can be normalized using the amount of platinum and are presented as mass activities (MA, mA g_{Pt}^{-1}). The metal compositions determined by XRF and electrodeposition efficiencies deduced in preliminary experiments for each of the studied systems on the basis of the applied charge and obtained mass are used for the normalizing.

Linear sweep voltammograms for the different catalysts are presented in Figure 5b. Figure 6 shows the relative activity of each electrodeposited catalyst compared to the commercial catalyst at potentials 0.6, 0.7 and 0.8 V vs. RHE. Figure 5b shows that for all the electrodeposited catalysts, the onset potential was shifted to more positive potential in comparison to the commercial catalyst and clearly higher activities are achieved at higher potential. Performances of Pt, PtCo and PtCu are similar before the cycling. Theoretically, Pt_3Ni surface should be highly active for ORR as shown by Rossmeisl *et al.* [41] but here PtNi is found to have a low activity. We presume that the applied synthesis method is not optimal for PtNi, although there is no clear difference between the electrochemical properties of cobalt and nickel that would explain this. However, XRD spectra (Figure 4) show weaker platinum peaks for PtNi which in this case could mean lower crystallinity or smaller crystal size as the electrodeposited metal loading is similar for all the samples.

During the cycling, the activities of all the electrodeposited catalysts decreased. However, PtCo experienced the smallest decrease in the activity as can be seen in Figure 6. Thus, according to the electrochemical and material characterization results, PtCo has the highest durability among the bimetallic catalysts and therefore, it is chosen for the laboratory-scale fuel cell experiments.

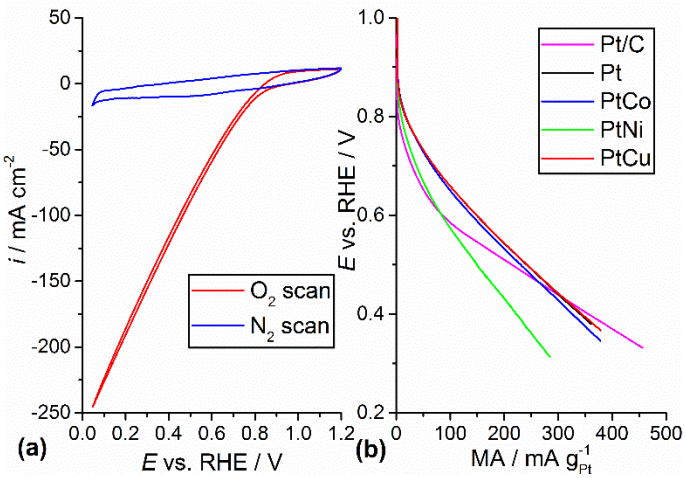

Figure 5. CVs of electrodeposited platinum in saturated oxygen and nitrogen with a scan rate of 50 mV s^{-1} (a) and ORR activities indicated in sweep voltammograms (5 mV s^{-1}) of the commercial reference material (Pt/C) and the different electrodeposited catalysts in a three-electrode cell (b).

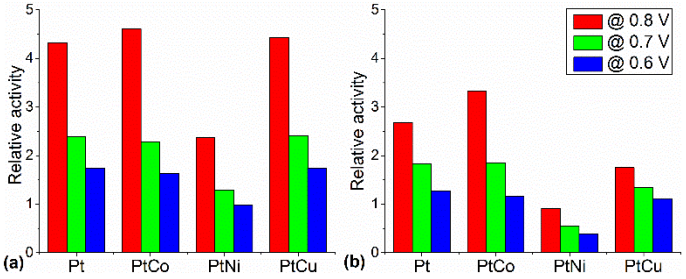

Figure 6. The relative ORR activities of electrodeposited catalysts normalized with respect to the commercial reference at different potentials vs. RHE before (a) and after (b) 3000 cycles.

3.3 Fuel cell experiments

Most of the research [24, 25, 26, 27, 18] done with electrodeposited catalysts for ORR has been performed by electrodeposition on RDE tip so that the interpretation of the data is straightforward and the effect of mass transfer can be separated. In this work, we utilize a more practical method for using these catalysts in a fuel cell. Earlier, Tominaka *et al.* [17] have been able to improve the ORR activity of palladium significantly by co-electrodeposition of PdCo. However, activity of PdCo is still far from that of platinum, onset potentials being 0.58, 0.68 and 0.73 V (vs. Ag/AgCl) for Pd, PdCo and Pt, respectively. We measured onset potentials of 0.86, 0.90, 0.89, 0.87 and 0.90 V (vs. RHE) for Pt/C, Pt, PtCo, PtNi and

PtCu, respectively. Wei *et al.* [28] have also a porous carbon electrode as a substrate for the electrodeposition. They used a dual-pulse current to deposit copper cores on the carbon and then immersed them in platinum containing solution to form a platinum layer by spontaneous galvanostatic replacement. Their measurements were also carried out in a conventional three-electrode cell and compared to a commercial Pt/C catalyst. Their results showed increased activities and an increase of approximately 0.05 V in the onset potential. For PtCo, Gasparatto *et al.* [36] have studied the effect of deposition potential and measured 50 % higher ORR activity for $Pt_{70}Co_{30}$ and 100 % higher for $Pt_{25}Co_{75}$ compared to pure platinum synthesized similarly.

The mesoporous PtCo catalyst was selected for fuel cell testing as it showed the highest durability. It was compared to a platinum catalyst prepared using the same method (Pt) and to a commercial platinum nanoparticle catalyst (20 *m* -% Pt, Alfa Aesar, Pt/C). For MEA characterization, impedance spectroscopy and cyclic voltammetry were used to characterize the cathode electrodes. For impedance, hydrogen was fed to cathode and oxygen to anode. For cyclic voltammograms, hydrogen was fed to the anode and nitrogen to the cathode so that the EASA of the cathode could be calculated based on hydrogen desorption. The measured parameters are presented in Table 5 and the impedance model circuit is presented in Figure 7. The first resistor, R_{el}, corresponds to all the resistances which are not related to the catalyst, i.e. cables, current collectors and the membrane of which the latter is most often the main source of this resistance. However, for the mesoporous electrodeposited materials, R_{el} is clearly higher that for Pt/C suggesting that dissimilar MEA preparation procedure results in high contact resistances for the former catalysts. The second resistor, R_{ct}, corresponds to the reaction kinetics of the studied electrocatalyst and the capacitor (which is modelled using a constant phase element) to the double layer capacitance of the electrocatalyst.

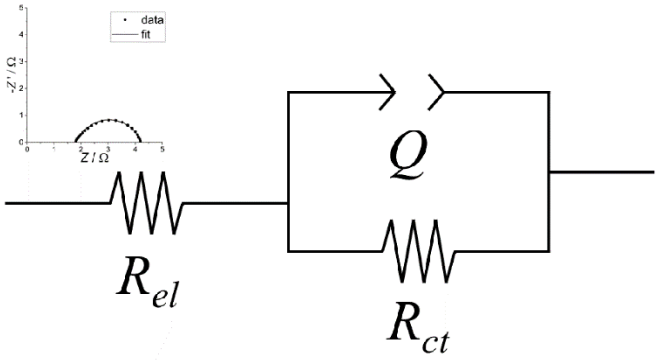

Figure 7. The electrical circuit used to model the impedance spectra.

During the cycling, the resistance of the Pt/C MEA increased slightly, whereas for the Pt and PtCo MEAs, it decreased by 50 % indicating notable improvement in the contact between the catalyst layer and the membrane with time. All the catalysts were activated during the cycling which can be observed as a decrease in the charge transfer resistance. The capacitance of the commercial catalyst is clearly higher than that of the electrodeposited catalysts due to the much higher area of the supporting carbon. EASA is initially much higher for the commercial catalyst but is decreased suggesting an aggregation of the nanoparticles. For the electrodeposited catalysts aggregation is less severe and therefore their EASA decreases only by 50 % of the original area. These results are in agreement with the BET observation made after durability measurements in the electrochemical cell (see Table 3 and the related discussion). When comparing electrodeposited Pt to PtCo, it can be observed that both resistances are higher for PtCo but on the other hand, it contains a lower amount of platinum.

Table 5. The parameters of the modelled circuit (Figure 7) for the measured impedance spectra and the EASAs determined by hydrogen desorption. The parameters are membrane resistance R_{el}, resistance correlated to the reaction kinetics R_{ct} and capacitance Q. Measurements were carried out at the beginning (1), after one day of cycling (2) and after one week of cycling (3).

Catalyst	R_{el} / Ω			R_{ct} / Ω			Q / mF			EASA / cm^2		
	1	**2**	**3**	**1**	**2**	**3**	**1**	**2**	**3**	**1**	**2**	**3**
Pt/C	0.97	0.86	1.18	2.89	2.08	0.86	211	259	248	2290	700	70
Pt	2.20	1.93	1.09	3.67	1.46	1.34	30	48	76	330	240	160
PtCo	2.86	1.83	1.51	4.41	2.41	2.00	26	31	38	370	230	180

To accelerate the degradation of the cathode catalyst potential of the DMFC was cycled within its operation range. Polarization curves measured at different stages, after one day and after one week of cycling, are presented in Figure 8. The pure platinum catalyst has a higher onset potential but at lower voltages the activity of PtCo is higher. It is also discovered that the activity of the commercial catalyst starts to decrease after cycling for 1−2 days, but for the electrodeposited catalysts the peak activity is reached after one week of cycling reflecting the changes observed in the impedance and EASA measurements. After the potential cycles, a 65 h constant voltage measurement was performed (Figure 8). During this period, the activity of all the studied catalysts decreases. These measurements show that the

electrodeposited mesoporous catalysts are slightly more active towards ORR in a DMFC and significantly more durable than the commercial platinum nanoparticle catalyst. This attributed to ability to retain the EASA and decrease of the contact resistance with time. Similar results have been published by Saejeng and Tantavichet [19] who have measured the effect of different electrodeposition parameters on the activity of PtCo nanoparticles in a fuel cell. They recorded an increase of 0.1 V in the cell voltage for a hydrogen fuel cell. A DMFC is used in our work, yet the relative voltage increase is similar.

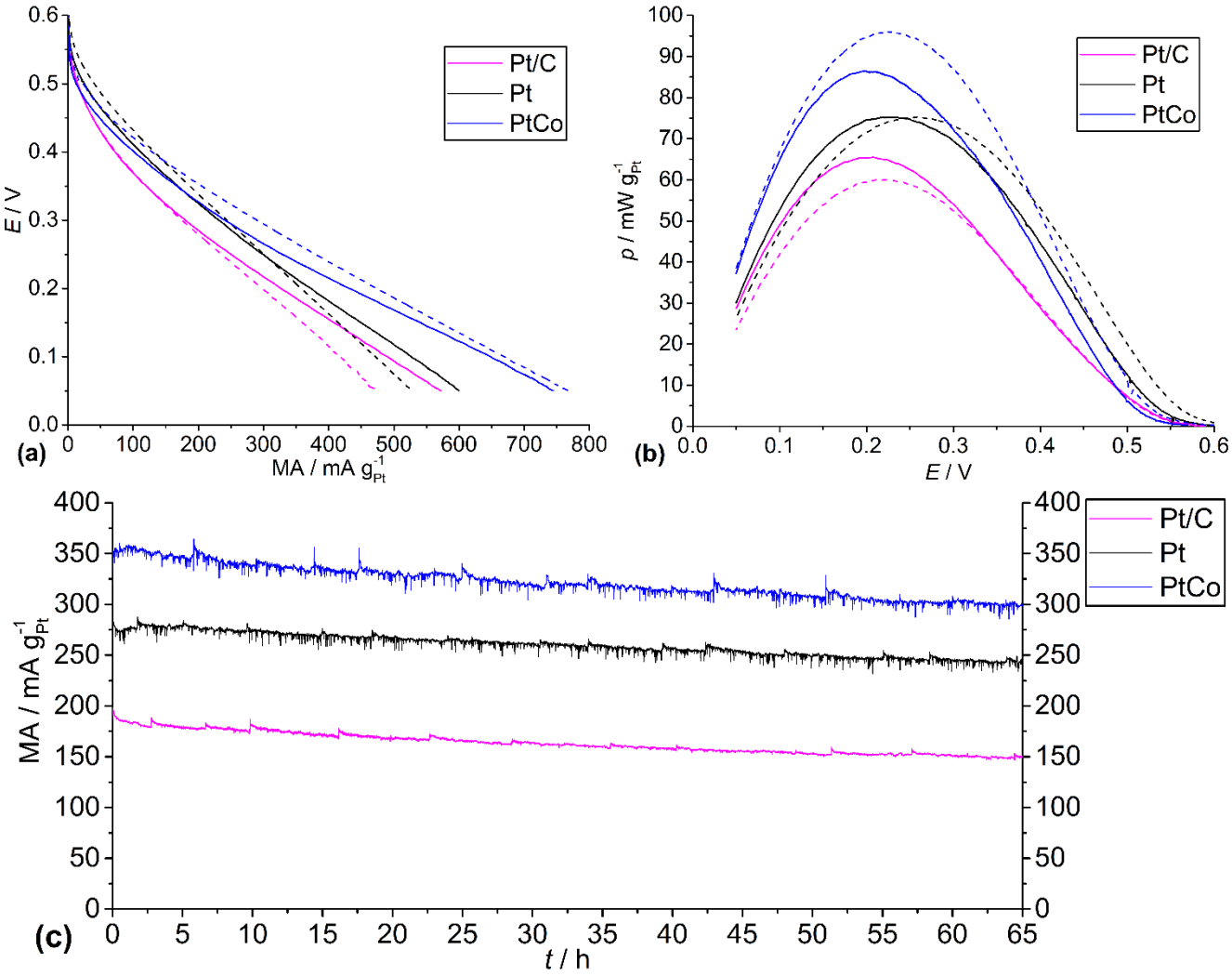

Figure 8. Above (a) polarization curves and (b) power curves and below (c) chronoamperometric measurements at 0.3 V in a MeOH/O_2 fuel cell at 70 °C. Solid lines correspond to initial measurements and dashed lines to measurements done after cycling.

4 Conclusions

PtCo, PtNi and PtCu bimetallic catalysts were successfully prepared by a single step electrodeposition process on a GDL-CT substrate. The catalysts activity and durability for ORR were investigated in an acidic media using a conventional three-electrode cell. Electrodeposited Pt, PtCo and PtCu showed an increased activity for ORR compared to commercial nanoparticular catalyst Pt/C. PtNi did not show high activities even though it has theoretically good surface properties for ORR. The BET measurements and BJH analysis showed that the structure of the catalyst is mesoporous and that the surface area decrease slower than for nanoparticular catalyst. PtCo showed the highest durability in the three-electrode tests and was further studied in a fuel cell. In the DMFC, PtCo showed clearly higher durability and activity when compared to both the similarly prepared Pt catalyst and a commercial catalyst. The method described in this study for synthesizing a fuel cell catalyst is practical, enabling the preparation of an MEA by directly combining two of these catalysts with a membrane. Liu and Pippel [18] have shown that electrodeposition of quaternary PtCoNiCu catalysts is possible, opening the option of further research to study the effect of combining multiple transition metals with platinum.

Acknowledgments

The authors would like to thank the Academy of Finland (the DEMEC, SUPER and CloseLoop projects) and Freeport Cobalt for funding this work. Also, Mr. Esko Ahvenniemi, Ms. Anne Tanskanen and Mr. Taneli Tiittanen are acknowledged for helping with the characterization and Ms. Nguyet Doan for helping with the synthesis. This study made use of the facilities of Aalto University Nanomicroscopy Center (Aalto-NMC).

References

[1] Lewis, N.S., Nocera, D.G., "Powering the planet: Chemical challenges in solar energy utilization," *P. Natl. Acad. Sci. USA,* 104 (2007) 15729-15735.

[2] Gasteiger, H.A., Kocha, S.S., Sompalli, B., Wagner, F.T., "Activity benchmarks and requirements for Pt, Pt-alloy, and non-Pt oxygen reduction catalysts for PEMFCs," *Appl. Catal. B,* 56 (2005) 9-35.

[3] F. J. Luczak and D. A. Landsman, "Noble metal-chromium alloy catalysts and electrochemical cell". Patent US Patent 4,316,944, 1982.

[4] F. J. Luczak and D. A. Landsman, "Ternary fuel cell catalysts containing platinum, cobalt and chromium". Patent US Patent 4,447,506, 1984.

[5] F. J. Luczak and D. A. Landsman, "Ordered ternary fuel cell catalysts containing platinum and cobalt and method for making catalysts". Patent US Patent 4,677,092, 1987.

[6] Mukerjee, S., Srinivasan, S., "Enhanced electrocatalysis of oxygen reduction on platinum alloys in proton exchange membrane fuel cells," *J. Electroanal. Chem.,* 357 (1993) 201-224.

[7] Mukerjee, S., Srinivasan, S., Soriaga, M.P., McBreen, J., "Effect of preparation conditions of Pt alloys on their electronic, structural, and electrocatalytic activities for oxygen reduction-XRD, XAS, and electrochemical studies," *J. Phys. Chem.,* 99 (1995) 4577-4589.

[8] Toda, T., Igarashi, H., Uchida, H., Watanabe, M., "Enhancement of the electroreduction of oxygen on Pt alloys with Fe, Ni, and Co," *J. Electrochem. Soc.,* 146 (1999) 3750-3756.

[9] Min, M., Cho, J., Cho, K., Kim, H., "Particle size and alloying effects of Pt-based alloy catalysts for fuel cell applications," *Electrochim. Acta,* 45 (2000) 4211-4217.

[10] He, T., Kreidler, E., Xiong, L., Luo, J., Zhong, C.J., "Alloy electrocatalysts combinatorial discovery and nanosynthesis," *J. Electrochem. Soc.,* 153 (2006) A1637-A1643.

[11] Stamenkovic, V.R., Mun, B.S., Arenz, M., Mayrhofer, K.J.J., Lucas, C.A., Wang, G., Ross, P.N., Markovic, N.M., "Trends in electrocatalysis on extended and nanoscale Pt-bimetallic alloy surfaces," *Nat. Mater.,* 6 (2007) 241-247.

[12] Zhong, C., Luo, J., Njoki, P.N., Mott, D., Wanjala, B., Loukrakpam, R., Lim, S., Wang, L., Fang, B., Xu, Z., "Fuel cell technology: nano-engineered multimetallic catalysts," *Energy Environ. Sci.,* 1 (2008) 454-466.

[13] Ammam, M., Easton, E.B., "Oxygen reduction activity of binary PtMn/C, ternary PtMnX/C (X = Fe, Co, Ni, Cu, Mo and Sn) and quaternart PtMnCuX/C (X = Fe, Co, Ni and Sn) alloy catalysts," *J. Power Sources,* 236 (2013) 311-320.

[14] Lai, F., Su, W., Sarma, L.S., Liu, D., Hsieh, C., Lee, J., Hwang, B., "Chemical dealloying mechanism of bimetallic Pt-Co nanoparticles and enhancement of catalytic activity towards oxygen reduction," *Chem. Eur. J.,* 16 (2010) 4602-4611.

[15] Shao, Y., Yin, G., Gao, Y., "Understanding and approaches for the durability issues of Pt-based catalysts for PEM fuel cell," *J. Power Sources,* 171 (2007) 558-566.

[16] Antolini, E., Salgado, J.R.C., Gonzalez, E.R., "The stability of Pt-M (M = first row transition metal) alloy catalysts and its effect on the activity in low temperature fuel cells," *J. Power Sources,* 160 (2006) 957-968.

[17] Tominaka, S., Momma, T., Osaka, T., "Electrodeposited Pd-Co catalyst for direct methanol fuel cell electrodes: Preparation and characterization," *Electrochim. Acta,* 53 (2008) 4679-4686.

[18] Liu, L., Pippel, E, "Low-platinum-content quaternary PtCuCoNi nanotubes with markedly enhanced oxygen reduction activity," *Angew. Chem. Int. Ed.,* 50 (2011) 2729-2733.

[19] Saejeng, Y., Tantavichet, N., "Preparation of Pt-Co alloy catalysts by electrodeposition for oxygen reduction in PEMFC," *J Appl Electrochem,* 39 (2009) 123-134.

[20] Attard, G.S., Göltner, C.G., Corker, J.M., Henke, S., Templer, R.H., "Liquid-crystal templates for nanostructured metals," *Angew. Chem. Int. Ed. Engl.,* 36 (1997) 1315-1317.

[21] Attard, G.S., Bartlett, P.N., Coleman, N.R.B., Elliott, J.M., Owen, J.R., Wang, J.H, "Mesoporous platinum films from lyotropic liquid crystalline phases," *Science,* 278 (1997) 838-840.

[22] Elliott, J.M., Attard, G.S., Bartlett, P.N., Coleman, N.R.B., Merckel, D.A.S., Owen, J.R., "Nanostructured platinum (H-ePt) films: Effects of electrodeposition conditions on film properties," *Chem. Mater,* 11 (1999) 3602-3609.

[23] Birkin, P.R., Elliott, J.M., Watson, Y.E., "Electrochemical reduction of oxygen on mesoporous platinum microelectrodes," *Chem. Commun.,* (2000) 1693-1694.

[24] Bauer, A., Wilkinson, D.P., Gyenge, E.L., Bizzotto, D., Ye, S., "Liquid crystalline phase templated platinum catalyst for oxygen reduction," *J. Electrochem. Soc.,* 156 (2009) B1169-B1174.

[25] Franceschini, E.A., Bruno, M.M., Viva, F.A., Williams, F.J., Jobbágy, M., Corti, H.R., "Mesoporous Pt electrocatalyst for methanol tolerant cathodes of DMFC," *Electrochim. Acta,* 71 (2012) 173-180.

[26] Kibsgaard, J., Gorlin, Y., Chen, Z., Jaramillo, T.F., "Meso-structured platinum thin films: Active and stable electrocatalysts for the oxygen reduction reaction," *J. Am. Chem. Soc.,* 134 (2012) 7758-7765.

[27] Doan, N., Sundqvist, T., Hiekkataipale, P., Korhonen, J., Kallio, T., Ruokolainen, J., Kontturi, K., Johans, C., "Electrodeposited mesoporous Pt and Pt@CB films as electrocatalysts for the oxygen reduction reactions and ethanol electrooxidation in both acid and alkaline media," *Int. J. Electrochem. Sci.,* 10 (2015) 2535-2553.

[28] Wei, Z.D., Feng, Y.C., Li, L., Liao, M.J., Fu, Y., Sun, C.X., Shao, Z.G., Shen, P.K., "Electrochemically synthesized Cu/Pt core-shell catalyst on a porous carbon electrode for polymer electrolyte membrane fuel cells," *J. Power Sources,* 180 (2008) 84-91.

[29] Nørskov, J.K., Rossmeisl, J., Logadottir, A., Lindqvist, L., Kitchin, J.R., Bligaard, T., Jónsson, H., "Origin of the overpotential for oxygen reduction at a fuel-cell cathode," *J. Phys. Chem. B,* 108 (2004) 17886-17892.

[30] Sanchez, J.M., Marán-López, J.L., Leroux, C., Cadeville, M.C., "Magnetic properties and chemical ordering in Co-Pt," *J. Phys.: Condens. Matter,* 1 (1989) 491-496.

[31] Dahmani, C.E., Cadeville, M.C., Sanchez, J.M., Marán-López, J.L., "Ni-Pt phase diagram: Experiment and theory," *Phys. Rev. Lett.,* 55 (1985) 1208-1211.

[32] Abe, T., Sundman, B., Onodera, H., "Thermodynamic assessment of the Cu-Pt system," *J. of Phase Equilib.,* 27 (2006) 5-13.

[33] Brunauer, S., Emmett, P.H., Teller, E., "Adsorption of Gases in Multimolecular Layers," *J. Am. Chem. Soc.,* 60 (1938) 309-319.

[34] Barrett, E.P., Joyner, L.G., Halenda, P.P., "The Determination of Pore Volume and Area Distributions in Porous Substances. I. Computations from Nitrogen Isotherms," *J. Am. Chem. Soc.,* 73 (1951) 373-380.

[35] Millazzo G., Caroli S., Sharma V.K., Tables of Standard Electrode Potentials, Chichester: John Wiley & Sons Ltd., 1978.

[36] Gasparotto, L.H.S, Ciapina, E.G., Ticianelli, E.A., Tremiliosi-Filho, G., "Electrodeposition of PVA-protected PtCo electrocatalysts for the oxygen reduction reaction in H2SO4," *J. Power Sources,* 197 (2012) 97-101.

[37] Strmcnik, D., Li, D., Lopes, P.P., Tripkovic, D., Kodama, K., Stamenkovic, V.R., Markovic, N.M., "When small is big: The role of impurities in electrocalysis," *Top. Catal.,* vol. 58, pp. 1174-1180, 2015.

[38] Qu, D., Shi, H., "Studies of activated carbons used in double-layer capacitors," *J. Power Sources,* 74 (1998) 99-107.

[39] Arblaster, J.W., "Crystallographic properties of platinum," *Platinum Met. Rev.,* 41 (1997) 12-21.

[40] Escudero-Escribano, M., Malacrida, P., Hansen, M.H., Vej-Hansen, U.G., Velázquez-Palenzuela, A., Tripkovic, V., Shiøtz, J., Rossmeisl, J., Stephens, I.E.L., Chorkendorff, I., "Tuning the activity of Pt alloy electrocatalysts by means of the lanthanide contraction," *Science,* 352 (2016) 73-76.

[41] Rossmeisl, J., Karlberg, G.S., Jaramillo, T., Nørskov, J.K., "Steady state oxygen reduction and cyclic voltammetry," *Faraday Discuss.,* 140 (2008) 337-346.